Fracture characteristics of high impact polystyrene under impact fatigue loadings

Taner Yilmaz · Tulin Sahin · Tamer Sinmazcelik

Abstract This study analyses the impact properties of high impact polystyrene (HIPS). HIPS is one of the well-known toughened polymers. The high toughness is given by the rubbery phase. The impact fatigue behavior of HIPS was studied with a Ceast pendulum type tester (Resil 25). The fracture mechanisms were examined with a scanning electron microscopy. The nature of crack initiation and propagation was investigated for small impact angles and three different spans. The impact angles of charpy hammer were chosen as 5°, 10°, 15°, 20°, and 25°. The fracture characteristics varied with the impact angle, the number of impacts, and the distance between supports. The rate of crack propagation was high at higher impact angles with lower endurance, and low at lower impact angles with higher endurance.

Introduction

Following the development of technology, industry is searching for lighter weight, higher strength, more efficient, and safer materials to meet the demands of structure design and economic benefits. Among these materials, plastics are the most promising. However, because of the limited strength and rigidity, plastics are difficult to design as structural parts [1].

Polymer toughness, in the form of impact resistance, is a measure of material or fabricated article ability to withstand the impact load without failure. Impact resistance is therefore a complex function of geometry, mode of loading, load application rate, environment (thermal and chemical), and material properties. The measured impact strength of a polymer must be the result of the sum of the contributions of all processes that dissipate as crack initiation and propagation process. Impact resistance is probably the most critical mechanical property of plastics, because it defines to the service life of the part, and involves the increasingly important matters of product safety and liability [2].

A process of adding rubbers to rigid plastics in order to increase their fracture resistance was first used commercially in 1948, with polystyrene being the matrix. The early success of high impact polystyrene (HIPS) led to the development of similar blends based on other rigid polymers, giving rise to the rubber-toughened grades, which are now available for most commercial plastics and thermosets of any significance [3–6]. Because HIPS is composed of multicomponent and multiphase polymeric materials, with glassy and rubbery phases, end-use properties are dependent on many variables, such as the composition and concentration, particle size, and particle size distribution of the rubber. It has been noticed that one of the main factors affecting the impact strength and toughness of HIPS is the rubber-phase particle size and its size distribution [7–11].

The fracture behavior of the resin component under load, with either single or repetitive loading conditions, particularly impact fatigue, has remained open for further investigation. There have been a few reported studies on the impact fatigue response of polymers. Rek et al. [12] studied dynamic mechanical behavior of styrene/butadiene copolymers and their blends. Ho et al. [1] studied the impact properties of a polycarbonate/acrylonitrile–butadiene–styrene blend. They found that the accumulation energy of impact fatigue was about 35–45 times higher

T. Yilmaz (✉) · T. Sahin · T. Sinmazcelik
Mechanical Engineering Department, Engineering Faculty,
Kocaeli University, Veziroglu Campus, Izmit 41040, Turkey
e-mail: taneryilmaz2002@yahoo.com

than for single impact. Suresh [13] examined the effect of repeated impacts on polymer surfaces in terms of heat generation and mechanochemical reactions. Ray et al. [14] investigated surface damage due to low velocity, angled impacts on vinylester. Şahin et al. [15] studied the effect of previous impact of HIPS at small falling angles.

The main purposes of this study are: (1) to analyze the repeated impact behavior, crack zone, crack initiation, and propagation mechanisms of the HIPS material, (2) to observe the impact fatigue fracture morphology through scanning electron microscopy (SEM), and (3) to make a comparative study between morphology of the surfaces that are fractured at different impact loadings.

Materials and methods

HIPS is a material produced as a result of reaction between butadiene synthetic elastomer and (5–14%) styrene containing crystal polymer in certain amounts. It is more resistant against impacts compared to unfilled polystyrene and also durable against organic liquids, liquid oils, and solid oils. Rubber-reinforced HIPS is manufactured by PETKIM (the Turkish petrochemical company) in granule form with a trade name of "Petren." The physical and mechanical properties of the material are given in Table 1. Standard test samples were produced in PETKIM by injection molding method. The samples were kept in controlled atmosphere that prevented from sunlight and humidity of the environment, till they are tested.

In this study, impact fatigue loading was performed through instrumented charpy impact tester. Samples are exposed to only impact tests before they are exposed to impact fatigue loading. Experiments were performed at different impact-energy values. It has been observed that there was no fracture on the surfaces of samples after the experiments performed with impact energy of 0.38 J (corresponds to impact angle of 25°). Because of that, we have done the fatigue-impact tests with energy values less than 0.38 J.

The samples were placed into the instrumented impact tester and struck with the pendulum hammer at small impact angles. These angles were chosen as 5°, 10°, 15°, 20°, and 25°. These impact energies of the strikes under these angles were corresponded to impact energy of 0.02, 0.06, 0.14, 0.24, and 0.38 J. The original distance between supports in standard charpy mode is 63.5 mm. However, in order to investigate the effect of span value, the distance between the supports were change to $L = 40$, 60, and 70 mm.

To determine the impact fatigue behavior, the samples were prepared according to ASTM D 256 standard. Notched samples with dimensions of $3.2 \times 12.7 \times 138 \text{ mm}^3$ were illustrated in Fig. 1. As shown in Fig. 1, SEM investigations were focused on A–D regions of the notched cross section of the charpy test samples.

Temperature and relative humidity values in laboratory atmosphere were measured as 23 °C and $50 \pm 10\%$, respectively. Instrumented charpy impact tests were performed on a Ceast pendulum type tester (Resil 25). A charpy hammer that has a strike range of 1.08 kN was used. Mass and length of the hammer was 1.254 kg and 0.327 m, respectively. Load and energy diagrams versus time and displacement were re-illustrated for each test.

During the impact achieved maximum force called as $F_{\max}$, which represents the crack initiation force. $X_{F_{\max}}$ represents the displacement occurred up to this point. The total energy (fracture energy) absorbed by the specimen until it fractures is defined as $E_{\max}$.

Experimental results

Figure 2 shows the impact fatigue test results performed at different impact energies. Although small variations exist due to the distances between the supports, as expected, the material fractured through small impact numbers in case of dropping the hammer from higher angles while lower drop angles required higher impact numbers. During the tests hammer permitted to hit the sample only one time at given

Table 1 Physical and mechanical properties of HIPS

Physical properties	Melting flow index (g/10 min) (200 °C, 5 kg)	2–5	ASTM D-238
	Vicat softening temperature (°C)	90	ASTM D-1525
	Heat bending temperature (°C)	80	ASTM D-648
	Glass transition temperature (°C)	90	ASTM D-638
Mechanical properties	Yield strength (daN/cm^2)	190	ASTM D-638
	Tensile strength (daN/cm^2)	220	ASTM D-638
	Tensile strain (%)	40–70	ASTM D-638
	Flexural strength (daN/cm^2)	400	ASTM D-790
	Flexural modulus (daN/cm^2)	1.7×10^4	ASTM D-790
	İzod impact strength (daN/cm^2)	8	ASTM D-256

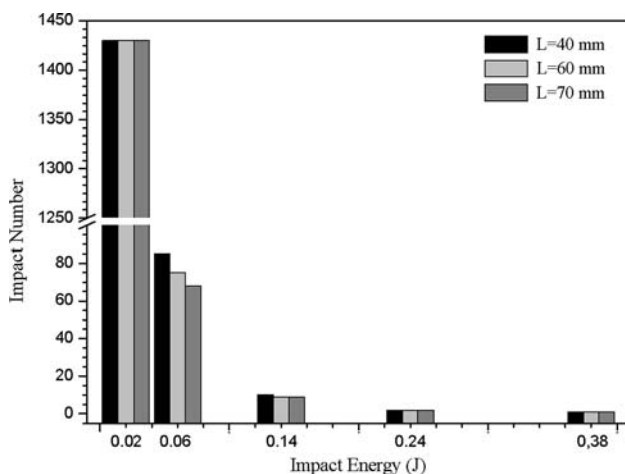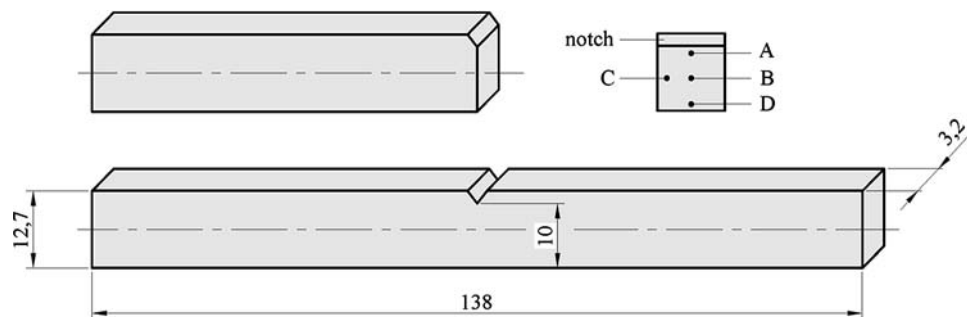Fig. 1 Geometry and location of A–D regions at the cross section of charpy impact sample

Fig. 2 Failure number depending on impact energy and the span (L)

Fig. 3 F_{max} variations for 0.14 J of impact energy

impact energy and the second hit was prevented. Samples were fractured after the impact number of approximately 1430 for 0.02 J (for each span values). On the other hand, the samples were fractured after less number of impacts as the distance between the supports (span) increased. Not surprisingly flexural displacement of the material, during the tests, increases as the distance between the supports increases. Therefore, the flexural stresses, and consequently deformations at crack tip also increase. As a result the impact number up to fracture was observed lower, as the distance between supports was longer.

Figure 3 shows the variations of obtained maximum forces during the impact fatigue study as a function of the span values while the impact energy is kept as constant at 0.14 J. In case of lowest span value (L = 40 mm), the samples was fractured after nine impacts. The sample behaved like a "more rigid" material compared to original because of the shorter span value, and therefore, higher F_{max} values are measured at this span compared to L = 60 and 70 mm. During the crack propagation in the material, the remaining cross section of the sample is decreased at each impact. Therefore, F_{max} value obtained from the actual impact was lower than the previous one. Samples tested at wider span values fractured at less number of impact cycles, because of higher bending moment values.
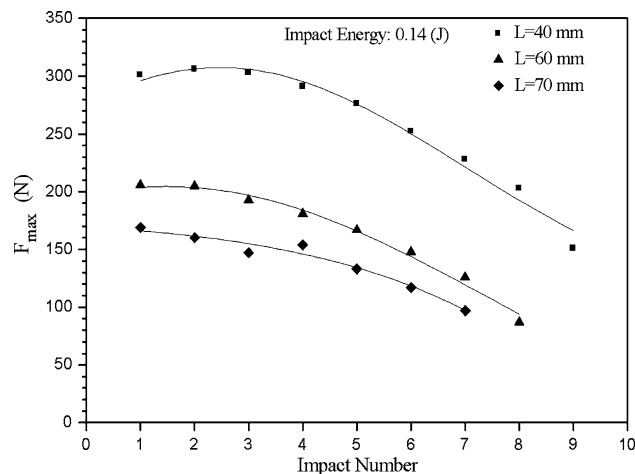
Variations in F_{max} for impact energy of 0.06 J were shown in Fig. 4. The results are very similar with the variations shown in Fig. 3. In Fig. 4, samples were fractured after higher impact numbers compared to Fig. 3. Also smaller span values give higher F_{max} values and higher impact number up to fracture. In Fig. 5, not surprisingly F_{max} values are quite lower compared to Figs. 3 and 4, also as expected the samples were fractured after high impact numbers. This phenomenon has also been observed in SEM examinations of the samples. In the case of higher impact angles, crack propagation lines were observed after each impact.

Figure 6 illustrates the variation of deformation rates as a function of impact number of the hammer. It is observed that crack propagation rate increases approximately in linear manner as a function of impacts, and failure occurs after the maximum deformation. As shown in Fig. 6, certain amount of deformation is achieved at smaller energy level impacts and larger number of loading cycles.

Figure 7 shows deformation rates as a function of impact numbers for impact energy of 0.02 J. At this low-energy value, crack propagates very slowly during each repeated impact. The curves of deformation rate (crack propagation rate) have three different regions similar to crack propagation behavior of the materials during fatigue
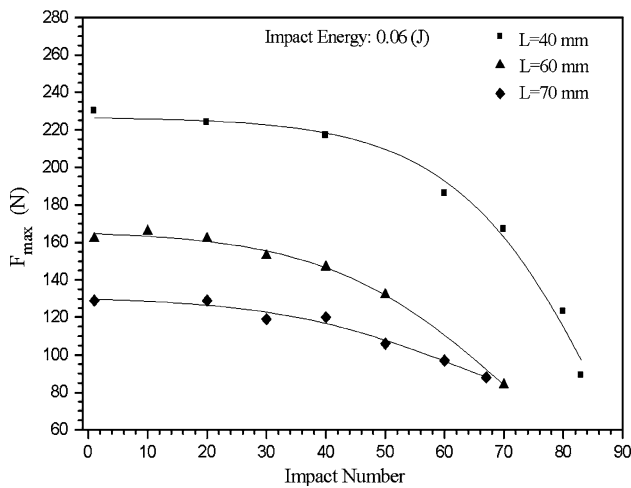
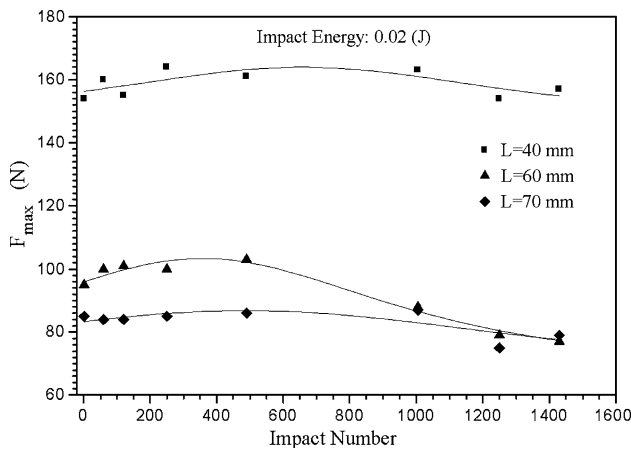Fig. 4 F_{max} variations for 0.06 J of impact energy

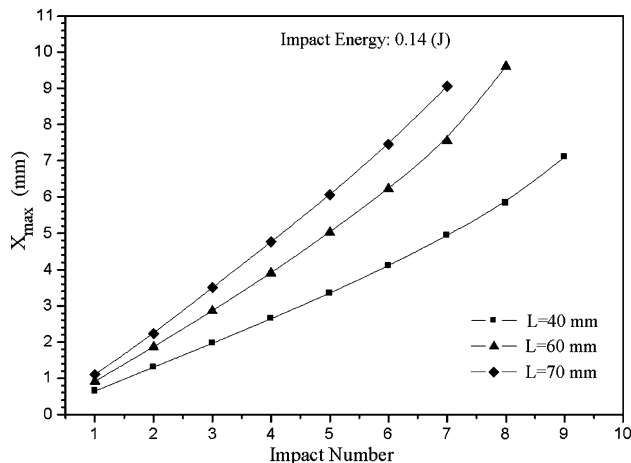Fig. 5 F_{max} variations for 0.02 J of impact energy

Fig. 6 X_{max} variations for 0.14 J of impact energy

loading. In region 1, it is observed that the deformation rate shows proportional increase with impact numbers up to 200–250. There is a high deformation rates observed in
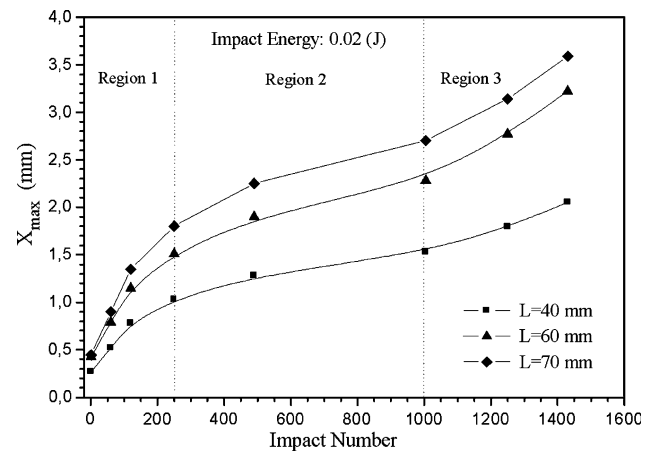

Fig. 7 X_{max} variations for 0.02 J of impact energy

region 1. On the other hand, between the 250 and 1000 impacts there is comparatively lower crack propagation rate. In region 3, the deformation rate increases, crack reaches its critical length and fracture occurs at the end of this region. Crack propagation was very limited during the repeated impacts of 0.02 J. Therefore, crack propagation lines did not occur in the structure. Decrease in F_{max} values of impact energy with 0.02 J was not as obvious as in the other impact energies for each span values. However, the crack propagated and failure occurred after approximately 1,400 impacts. The fact that no variation occurred in force values during crack propagation indicates that plastic zone and stiffening formed on crack tip produced a strong resistance against every next impact.

Figure 8 shows SEM micrographs taken from the materials' cross sections, which are fractured after repeated impacts. At the left hand side, image represents the fracture surface of the sample fractured with repeated impacts of 0.02 J. Considering the cross section of the fractured material, it is seen that higher plastic deformation traces exist on the cross sections compared with other fractured samples with higher hammer energies. The cross section does not seem like there was planar crack propagation. Crack propagation line formation was not observed. Crack propagation lines are clearly visible on the sample's cross section of the fractured sample after repeated impacts of 0.06 J. The notch, which was produced by machining, is seen on the upper sides of the images. Crack propagation direction is from top toward down of the sample. It was observed that crack propagation lines at notch tip are closer to each other and the distance between them became longer after each impact. It was also observed that the distance between these lines, which occurred before final failure, became fairly longer. Higher repeated impact energies give longer distance between the crack propagation lines. This phenomenon can be clearly observed in Fig. 8. In addition, amount of crack propagation increases toward the edge of

Fig. 8 Fracture surface of the sample under different repeated impact energies (span = 60 mm)

(5°-0.02 J)   (10°-0.06 J)   (15°-0.14 J)   (20°-0.24 J)   (35°-0.38 J)
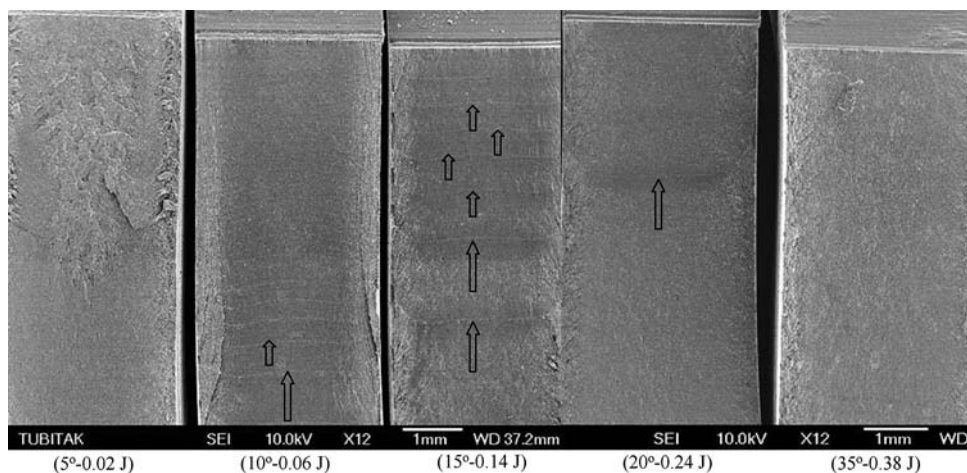
the samples. The specimen was fractured after two repeated hammer impacts with impact energy of 0.24 J. According to the surface examinations after failure, the only one crack propagation line occurred on the cross section is seen clearly. The cross section of the sample fractured with single impact, and impact energy of 0.38 J is shown in Fig. 8. No crack propagation line exists on the cross section because the sample was fractured with single impact.

Figure 9 illustrates the "region A" of the fractured sample with repeated impacts of 0.02 J. As mentioned above, crack propagation lines were not observed on the cross section of the fracture surface. In the figure, typical ductile fracture morphology is clearly shown. There is high plastic deformation in the cross-sectioned region of the sample.

Figure 10 illustrates the same fractured region under high magnification. It is observed from the image that the crack propagated through the particles. The diameter of the particles varies between 2 and 10 μm, and their distribution is clearly seen at the cross section of the fracture surface.

Figure 11 represents the 10,000× magnification of "region A." Note that the crack propagates with smallest impact energy of 0.02 J. The spherical elastomeric particles are not debonded and there are not any observed deformations.

In Fig. 12, "region B" represents the middle of fractured cross section of the sample. As implied above, the crack propagation rate is faster at "region B" compared to "region A." The higher crack propagation velocity results in deformations in the spherical particles, and higher matrix deformations are observed compared to "region A." White-colored texture implies that there is large amount of deformation in the elastomeric particles and the matrix material.

Figure 13 illustrates the "region A" of the cross section of fractured sample with repeated impacts of 0.06 J. Magnification ratios on Figs. 10 and 13 are the same.
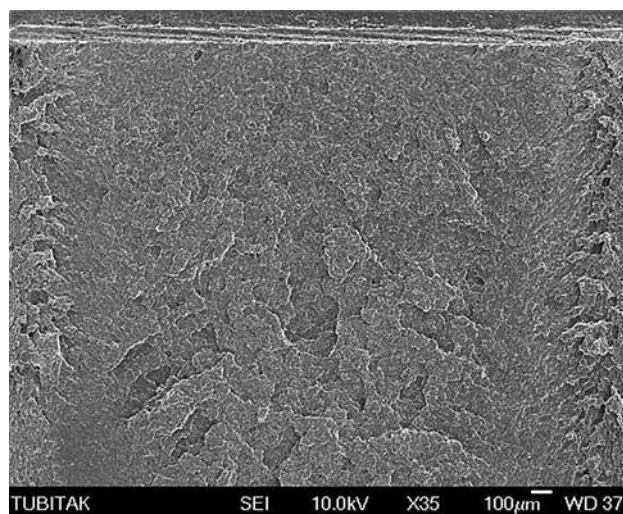

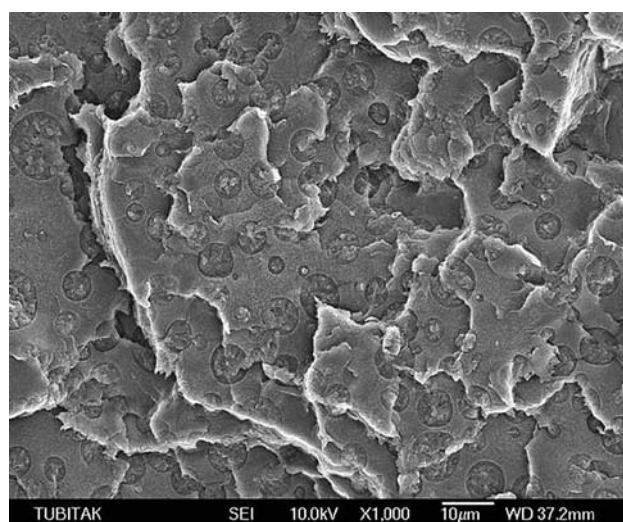**Fig. 9** Region A in case of $L = 60$ mm and 0.02 J

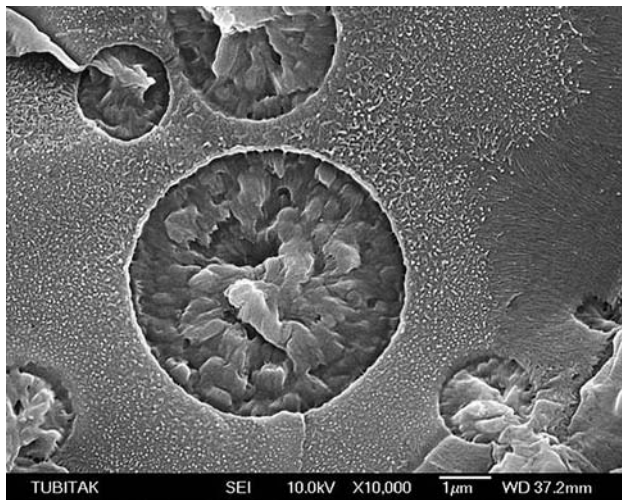**Fig. 10** Region A in case of $L = 60$ mm and 0.02 J (at high magnification)

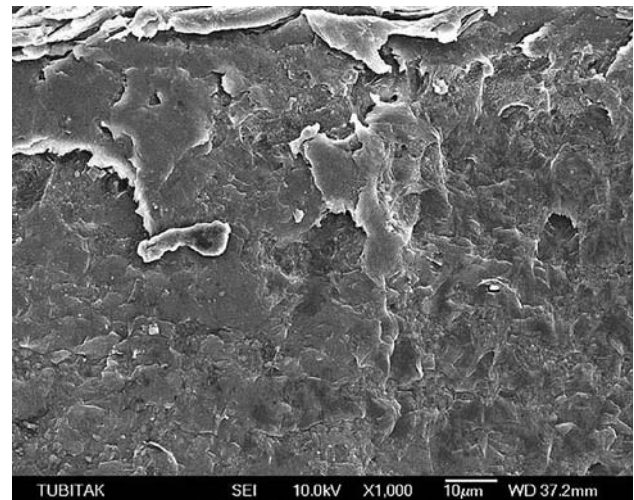**Fig. 11** Region A in case of $L = 60$ mm and 0.02 J (magnification is 10,000×)

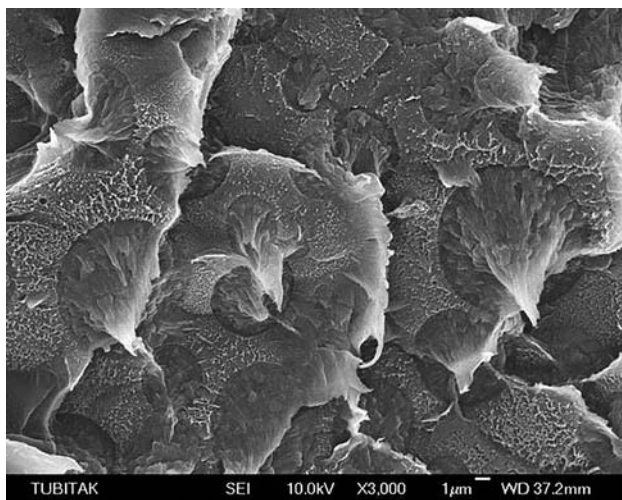**Fig. 13** Region A in case of $L = 60$ mm and 0.06 J

Fig. 12 Region B in case of $L = 60$ mm and 0.02 J
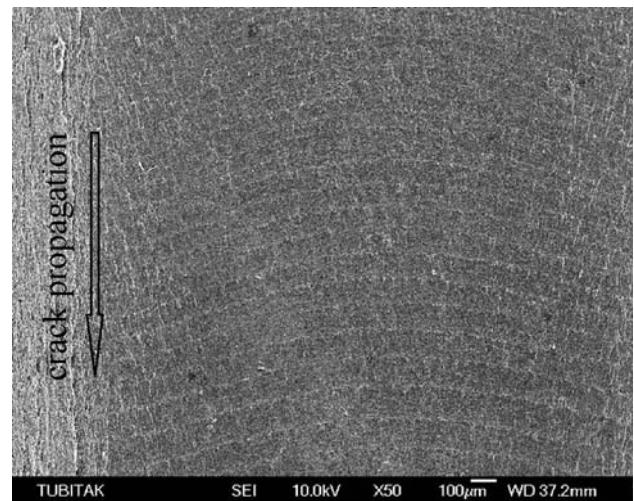

Fig. 14 Region B in case of $L = 60$ mm and 0.06 J

However, impact energy of the hammer is three times higher in Fig. 13 compared with Fig. 10. Although the spherical butadiene particles are seen on the fractured cross section of the sample in Fig. 10, but these particles are not seen on the fractured surface in Fig. 13. The fractured surface in Fig. 13 is rougher than the surface in Fig. 10. Since cracks propagate inside the matrix material, or matrix–particle interface, or around the particles without passing through the particles, energy absorption during crack propagation is reduced. As a result, brittle type of fracture with lower energy absorption is generated.

Figure 14 illustrates the "region A" of the cross section of the sample fractured after repeated impacts of 0.06 J. It is seen that the distance between crack propagation lines is extending at each impact. It has been observed that crack propagation distance increases toward the edge of the test sample.

Figure 15 illustrates the SEM image taken from between B and D regions. This micrograph also shows that the distance between crack propagation lines extending from small ranges to gradually longer ones. The distance between these lines is approximately 100 μm on upper sides of the region while it reaches up to 300 μm toward to lower sides of the region. The cracks are in the form of rough arches on the upper sides of the region. On the other hand, it is seen that the crack tips propagate faster at the left and right edges (arrows 1 and 2) of the sample compared with the center of the sample (arrow 3).

Figure 16 illustrates the last two crack propagation lines in "region D" of the fractured sample. The distance between the last two crack propagation lines is approximately 1000 μm. Crack propagation velocity is still lower at central region of the failure surface compared to edges.
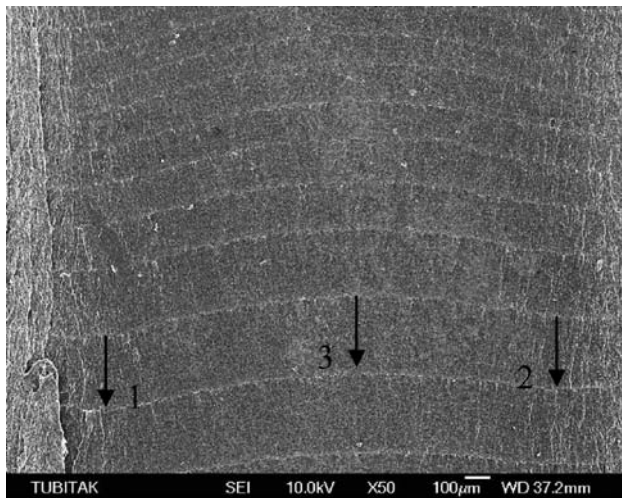
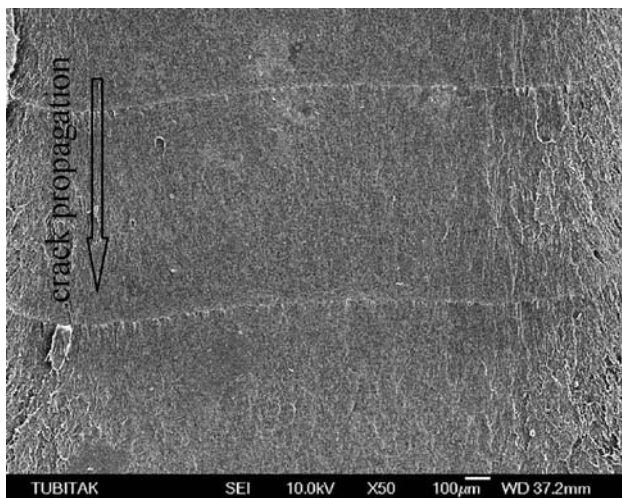**Fig. 15** Regions B–D in case of $L = 60$ mm and 0.06 J

Fig. 16 Region D in case of $L = 60$ mm and 0.06 J

Conclusion

As a result of repeated impacts, many changes occurred within the material. These changes concentrated at the crack tip and the fracture surface. There are remarkable structural and geometrical changes at the notch tip. These are summarized as notch tip radius changes, changes of the crack shape, crazing, and plastic zone formation at the crack tip. Structural and geometrical changes at the notch

tip in the material are proportional with the magnitude of the previous impact. Repeated impacts, over a certain number, result in higher crack propagation velocity and catastrophic failure. The crack produced by impact loadings, similar to fatigue during dynamic loading, propagates and consequently causes failure in the material. Magnitude of the impacts applied on the material strongly affects fracture morphology.

The main results from this study are:

1. For each span values, samples were fractured after the impact number of nearly 1430 for 0.02 J.
2. While the impact energy is kept as constant at 0.14 J, the samples were fractured after nine impacts and higher F_{max} values are measured due to the shortest span value.
3. Lower impact energies give lower F_{max} values, shorter crack propagation distance, and higher impact numbers up to fracture. Failure occurred when crack propagation velocity reached its maximum value.

References

1. Ho MH, Hwang JR, Doong JL (1999) Polym Eng Sci 39:708
2. Perkins WG (1999) Polym Eng Sci 39:2445
3. Trantina G, Nimmer R (1994) Structural analysis of thermoplastic components. McGraw-Hill, New York, p 241
4. McCrum NG, Buckley CP, Bucknall CB (1997) Principles of polymer engineering. Oxford Science Publications, New York, p 84
5. Strong AB (2000) Plastics: material and processing. Prentice Hall, NJ, p 143
6. Argon AS (1999) J Appl Polym Sci 72:13
7. Turley SG, Keskkula H (1980) Polymer 21:466
8. Lee SJ, Jeoung HG, Ahn KH (2003) J Appl Polym Sci 89:3672
9. Dagli G, Argon AS, Cohen RE (1995) Polymer 36:2173
10. Rios-Guerrero L, Keskkula H, Paul DR (2000) Polymer 41:5415
11. Jelcic Z, Holjevac-Grguric T, Rek V (2005) Polym Degrad Stab 90:295
12. Rek V, Holjevac-Grguric T, Jelcic Z, Hace D (1999) Macromol Symp Polym Charact 148:425
13. Suresh S (1999) Fatigue of materials; Cambridge solid state science series. Cambridge University Press, Cambridge, UK, p 192
14. Ray D, Sarkar BK, Bose NR (2002) J Appl Polym Sci 86:1995
15. Şahin T, Sinmazçelik T, Arici A (2004) J Mater Sci 39:2543. doi: 10.1023/B:JMSC.0000020024.52958.13